

This is a copy of the published version, or version of record, available on the publisher's website. This version does not track changes, errata, or withdrawals on the publisher's site.

# Effect of overlapping laser beams and density scale length in laser-plasma instability experiments on OMEGA EP

M. J. Rosenberg, A. A. Solodov, J. F. Myatt, S. Hironaka, J. Sivajeyan, R. K. Follett, T. Filkins, A. V. Maximov, C. Ren, S. Cao, P. Michel, M. S. Wei, J. P. Palastro, R. H. H. Scott, K. Glize, and S. P. Regan

## Published version information

**Citation:** MJ Rosenberg et al. Effect of overlapping laser beams and density scale length in laser-plasma instability experiments on OMEGA EP. *Phys Plasmas* 30, no. 4 (2023): 042710

**DOI:** [10.1063/5.0135603](https://doi.org/10.1063/5.0135603)


This article may be downloaded for personal use only. Any other use requires prior permission of the author and AIP Publishing. This article appeared as cited above.

This version is made available in accordance with publisher policies. Please cite only the published version using the reference above. This is the citation assigned by the publisher at the time of issuing the APV. Please check the publisher's website for any updates.

This item was retrieved from **ePubs**, the Open Access archive of the Science and Technology Facilities Council, UK. Please contact [epublications@stfc.ac.uk](mailto:epublications@stfc.ac.uk) or go to <http://epubs.stfc.ac.uk/> for further information and policies.

RESEARCH ARTICLE | APRIL 10 2023

## Effect of overlapping laser beams and density scale length in laser-plasma instability experiments on OMEGA EP

M. J. Rosenberg ; A. A. Solodov; J. F. Myatt; ... et. al



*Physics of Plasmas* 30, 042710 (2023)

<https://doi.org/10.1063/5.0135603>



CrossMark

### Articles You May Be Interested In

Identification of stimulated Raman side scattering in near-spherical coronal plasmas on OMEGA EP

*Physics of Plasmas* (February 2023)

Hydrodynamic simulations of long-scale-length two-plasmon–decay experiments at the Omega Laser Facility

*Physics of Plasmas* (March 2013)

Implementation of a Wollaston interferometry diagnostic on OMEGA EP

*Rev Sci Instrum* (August 2018)

# Effect of overlapping laser beams and density scale length in laser-plasma instability experiments on OMEGA EP

Cite as: Phys. Plasmas **30**, 042710 (2023); doi: 10.1063/5.0135603

Submitted: 21 November 2022 · Accepted: 27 March 2023 ·

Published Online: 10 April 2023



View Online



Export Citation



CrossMark

M. J. Rosenberg,<sup>1,a)</sup> A. A. Solodov,<sup>1</sup> J. F. Myatt,<sup>2</sup> S. Hironaka,<sup>2</sup> J. Sivajayan,<sup>2</sup> R. K. Follett,<sup>1</sup> T. Filkins,<sup>1</sup> A. V. Maximov,<sup>1</sup> C. Ren,<sup>3</sup> S. Cao,<sup>3</sup> P. Michel,<sup>4</sup> M. S. Wei,<sup>1</sup> J. P. Palastro,<sup>1</sup> R. H. H. Scott,<sup>5</sup> K. Glize,<sup>5</sup> and S. P. Regan<sup>1</sup>

## AFFILIATIONS

<sup>1</sup>Laboratory for Laser Energetics, University of Rochester, Rochester, New York 14623, USA

<sup>2</sup>Department of Electrical and Computer Engineering, University of Alberta, Edmonton, Alberta T6G1H9, Canada

<sup>3</sup>University of Rochester, Rochester, New York 14623, USA

<sup>4</sup>Lawrence Livermore National Laboratory, Livermore, California 94550, USA

<sup>5</sup>Central Laser Facility, STFC Rutherford Appleton Laboratory, Harwell Oxford, Didcot OX11 0QX, United Kingdom

<sup>a)</sup>Author to whom correspondence should be addressed: [mros@lle.rochester.edu](mailto:mros@lle.rochester.edu)

## ABSTRACT

Experiments have been conducted on the OMEGA EP laser facility to study the effect of density scale length and overlapping beam geometry on laser-plasma instabilities near and below the quarter-critical density. Experiments were conducted in both planar geometry (density scale length  $L_n \sim 190$  to  $300 \mu\text{m}$ ) and spherical geometry ( $L_n \sim 150 \mu\text{m}$ ) with up to four overlapping beams and were designed to have overlapped intensities and density scale lengths comparable to OMEGA spherical experiments, but with many fewer beams. In comparison with previous experiments on OMEGA and National Ignition Facility, it is confirmed that shorter density scale lengths favor the two-plasmon decay (TPD) instability, while longer density scale lengths favor stimulated Raman scattering (SRS). In addition, for experiments at the same scale length and overlapped laser intensity, higher single-beam intensities favor SRS, while a larger number of overlapping beams favor TPD.

Published under an exclusive license by AIP Publishing. <https://doi.org/10.1063/5.0135603>

## I. INTRODUCTION

Laser-plasma instabilities (LPI)<sup>1</sup> are a concern in laser-based inertial confinement fusion (ICF)<sup>2</sup> experiments because of the reduction in laser energy coupled to the target, impacts on drive symmetry, and the potential generation of hot electrons, which can limit compression of the imploding capsule. Stimulated Raman scattering (SRS)<sup>3–5</sup> and two-plasmon decay (TPD)<sup>6</sup> can occur at densities near the quarter-critical density of the laser [ $n_e = n_c/4$ , where  $n_e$  is the electron density and  $n_c$  is the critical density for the laser wavelength  $\lambda_0$  (in  $\mu\text{m}$ ), with  $n_c \approx 1.1 \times 10^{21} \lambda_0^{-2} \text{cm}^{-3}$ ] and have been observed in laser-plasma experiments at intensities relevant to ICF. SRS can also be driven at densities below quarter-critical. Understanding these instabilities and their dependence on density scale length, plasma temperature, and overlapping laser beam geometry is critical to the pursuit of ICF ignition and fusion gain on facilities such as the National Ignition Facility (NIF).<sup>7</sup>

Previous experiments have demonstrated the prevalence of TPD<sup>8</sup> in 60-beam direct-drive<sup>9</sup> ICF implosions at density scale lengths  $L_n \sim 150 \mu\text{m}$  and electron temperatures  $T_e \sim 2 \text{keV}$  on the OMEGA laser.<sup>10</sup> Likewise, planar- and spherical-geometry direct-drive experiments on the NIF<sup>11–13</sup> have shown the predominance of SRS at  $L_n \sim 400$ – $600 \mu\text{m}$  and  $T_e \sim 4.5 \text{keV}$  with varying numbers of overlapping beams.

To complement this dataset, planar and spherical experiments were designed on OMEGA EP<sup>14</sup> to explore systematically intermediate scale lengths and to assess the effect of overlapping laser geometry on LPI mechanisms. Relative to OMEGA, OMEGA EP offers advantages of higher single-beam laser energies, which enable both higher single-beam intensities and longer laser pulses to drive longer scale length conditions in planar geometry. While previous experiments on OMEGA EP explored the effect of different overlapped laser conditions on hot electron production, no scattered light spectral diagnostics

were available to infer LPI mechanisms and TPD was assumed to be responsible.<sup>15</sup> In contrast, the experiments reported here measured scattered light spectra and show both SRS and TPD, even at scale lengths that on OMEGA produced only TPD. These results indicate, in accordance with theory,<sup>16,17</sup> that SRS is sensitive to high single-beam intensities or long scale lengths, while TPD is more strongly driven by many overlapping beams.

This paper is organized as follows: The experimental setup for OMEGA EP experiments and simulations thereof are discussed in Sec. II. LPI scattered light measurements showing evidence of SRS and TPD are presented in Sec. III. A comparison to previous data on OMEGA and NIF, showing the effects of scale length and beam overlap, as well as LPI threshold considerations consistent with the data, is discussed in Sec. IV. Concluding remarks and potential implications for direct drive ICF are presented in Sec. V.

## II. EXPERIMENTAL SETUP AND SIMULATIONS

LPI experiments on OMEGA EP used spherical or planar CH targets, irradiated on one side by up to four 351 nm laser beams at angles of 23.2° relative to the axis of symmetry (Fig. 1). The spherical experiments used solid spheres with a nominal diameter of 700 μm, while the planar experiments used planar slab targets with a thickness of 250 μm and a width of 3 to 4 mm, several times larger than the laser spot [Figs. 1(a) and 1(b)]. On four-beam experiments, a total laser energy of 8.2 to 9.3 kJ was used, either in a 2-ns square pulse or a 4-ns linear ramp pulse [Fig. 1(c)], with a peak power of around 4 TW. The beam spots were defined by distributed phase plates (DPPs), with a nominal diameter of either 750 μm (super-Gaussian of order 8.9 with 1/e radius of 336 μm) or 400 μm (super-Gaussian of order 16.7 with 1/e radius of 233 μm). The laser beams were designed to perfectly overlap close to the quarter-critical surface, near where LPI takes place, and were pointed either 200 μm in front of the target for planar experiments or toward the center of the sphere for spherical experiments. There was a small amount of laser blowby (light from the periphery of the beams refracting past the target) on the spherical experiments, where the 750 μm spot size overfilled the 700 μm target, which contributes to the generation of SRS sidescatter.<sup>18–20</sup> Some single-beam experiments were performed, with the total energy, power, and intensity reduced accordingly by a factor of four.

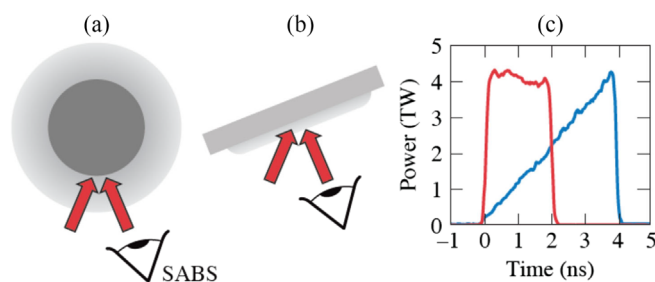


**FIG. 1.** Experimental geometry for LPI experiments on OMEGA EP, using (a) 700-μm diameter spherical CH targets and (b) 250-μm thick planar CH targets. The time-resolved SRS diagnostic SABS was located in the Beam 4 beamline. Some experiments used four beams at angles of 23.2° relative to their common symmetry axis, while others used only Beam 4. Either (c) 2-ns square pulses (red) or 4-ns linear ramp pulses (blue) with a peak power of 4 TW were used.

The planar targets were oriented normal to Beam 4, which contains the sub-aperture backscatter station (SABS) diagnostic.<sup>21</sup> SABS samples multiple regions of the beam aperture, using optical fibers to pick off a portion of the scattered light to be relayed to a spectrometer and an optical streak camera to capture the time-resolved scattered light at wavelengths of 400 to 750 nm, including scattered light from both SRS and TPD. This target orientation particularly favors collection of scattered light near 702 nm from the quarter-critical density region, which is only observed within ~10° of target normal.<sup>22</sup> Single-beam experiments reported here used Beam 4.

Two-dimensional (2D) DRACO<sup>23</sup> radiation-hydrodynamics simulations were used to calculate the plasma conditions. DRACO simulations were performed in cylindrically symmetric R–Z geometry with the Z axis directed along the beam symmetry axis. DRACO simulations include 3D laser ray trace<sup>24</sup> (with azimuthal symmetry for energy deposition as appropriate for an axisymmetric code), non-local electron thermal transport,<sup>25,26</sup> and multi-group diffusion radiation transport with Los Alamos astrophysical opacity tables.<sup>27</sup> Cross-beam energy transfer was not included in these simulations, though this is expected to be negligible with all drive beams incident on the same side of the target. The simulations (Fig. 2) provide calculated time-dependent local density scale length, electron temperature, overlapped laser intensity, and threshold parameters ( $\eta$ ) for the absolute TPD or absolute SRS backscatter instabilities<sup>6,28</sup> based on overlapped laser intensity at the quarter-critical density along the axis of symmetry for a planar experiment [Figs. 2(a)–2(d)] and a spherical experiment [Figs. 2(e)–2(h)] with 750 μm DPPs and a 2-ns square pulse. The respective threshold parameters are defined as  $\eta_{\text{TPD}} = I/I_{14}^{\text{TPD,thr}}$  and  $\eta_{\text{SRS}} = I/I_{14}^{\text{SRS,thr}}$ , where  $I$  is the total overlapped laser intensity and  $I_{14}^{\text{TPD,thr}} = 233 T_{e,\text{keV}}/L_{n,\mu\text{m}}$  and  $I_{14}^{\text{SRS,thr}} = 2377/L_{n,\mu\text{m}}^{4/3}$  are the intensity thresholds (units of  $10^{14}$  W/cm<sup>2</sup>) for absolute TPD and SRS backscatter at quarter-critical density. The single-beam threshold parameter in four-beam experiments can be considered to be these threshold parameters divided by 4. The 2D variation in electron density in directions both parallel and perpendicular to the target surface is shown for the spherical experiment in Fig. 2(i). The assumption of azimuthal symmetry is valid, modulo the fourfold beam pattern, for the spherical experiments. For the planar experiments, DRACO does not account for the 23.2° tilt of the target relative to the beam symmetry axis in order to face Beam 4. This is considered a small perturbation.

Planar experiments with four beams were predicted to reach density scale lengths on axis of around 300 μm, electron temperatures of 2.8 keV, and overlapped laser intensities of  $8 \times 10^{14}$  W/cm<sup>2</sup> at the quarter-critical density. In contrast, the spherical four-beam experiments were predicted to achieve radial scale lengths of only 150 μm, but similar peak electron temperatures (2.7 keV) and overlapped laser intensities at  $n_c/4$  ( $8.5 \times 10^{14}$  W/cm<sup>2</sup>). The difference in scale length between planar and spherical experiments largely drives the difference in TPD and SRS threshold parameters calculated based on overlapped laser intensity. Likewise, the balance between  $\eta_{\text{SRS}}$  and  $\eta_{\text{TPD}}$  is different, with the longer-scale length planar experiments favoring absolute SRS, while the shorter-scale length spherical experiments are closer to equally favorable for SRS and TPD when the total overlapped intensity is considered. The consideration of single-beam intensities when evaluating proximity to TPD and SRS thresholds is discussed in Sec. IV. Similar plasma conditions are predicted at the end of the laser pulse in

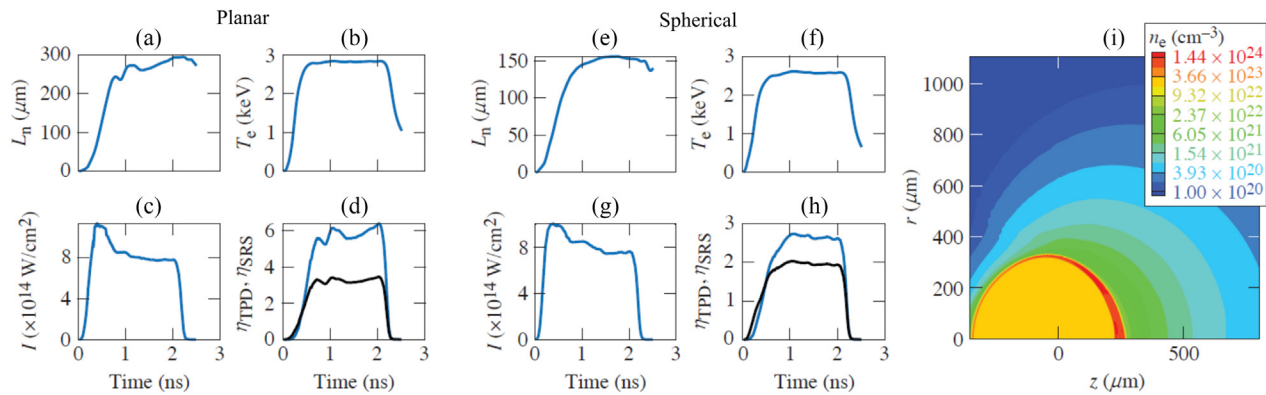


**FIG. 2.** 2D DRACO-simulated plasma conditions at the quarter-critical density along the axis of symmetry for four-beam experiments driven by a 2-ns square pulse in either (a)–(d) planar geometry (shot 27108, which used a planar target normal to the OMEGA EP beam symmetry axis with the same laser drive as on experiments normal to Beam 4) or (e)–(i) spherical geometry. The density scale length [(a) and (e)], electron temperature [(b) and (f)], overlapped laser intensity [(c) and (g)], and SRS (blue) and TPD (black) threshold parameters  $\eta$  [(d) and (h)] are shown. Simulated 2D density contours in the spherical experiment (i) at  $t = 1.25$  ns show the deviation from spherical symmetry in the lateral direction (laser beams incident from the right at  $23.2^\circ$  from the  $z$  axis).

ramp-pulse experiments. Planar experiments using a single beam with the same  $750 \mu\text{m}$  phase plate have an intensity reduced by a factor of  $\sim 4$  and consequently lower electron temperature (1.7 keV) and density scale length ( $220 \mu\text{m}$ ). A single-beam planar experiment using the  $400 \mu\text{m}$  phase plate and, therefore, a smaller beam spot produced a  $190 \mu\text{m}$  scale length, and a laser intensity ( $4 \times 10^{14} \text{ W/cm}^2$ ) between the overlapped laser intensity for large-spot single-beam and four-beam cases, but consequently a much higher single-beam intensity than either.

### III. RESULTS

Time-resolved scattered light spectra between wavelengths of 400 and  $750 \text{ nm}$  were measured for a variety of experiments driven by the 2-ns square pulse. Figure 3 summarizes the data, obtained on (a) a planar experiment driven by four beams with  $750\text{-}\mu\text{m}$  spots, [(b) and (c)] planar experiments driven by a single  $750\text{-}\mu\text{m}$  beam, (d) a planar experiment driven by a single  $400\text{-}\mu\text{m}$  beam, and (e) a  $700\text{-}\mu\text{m}$ -diameter spherical target driven by four beams with  $750\text{-}\mu\text{m}$  spots. Different neutral density filters, apertures, and overall SABS throughput limit the comparison of absolute signal levels between experiments, though the comparison of relative prominence of different features in the spectra is valid.

The data show the relative importance of TPD and SRS signatures. TPD is evident in a doublet feature corresponding to half-harmonic ( $\omega/2$ ) centered around a wavelength ( $702 \text{ nm}$ ) twice the incident laser wavelength, emitted from the quarter-critical region.<sup>29</sup> In contrast, SRS appears sometimes as a singlet redshifted  $\omega/2$  feature from absolute SRS backscatter at quarter-critical density,<sup>11</sup> as well as a broad-wavelength feature  $< 680 \text{ nm}$  generated by SRS in the underdense ( $n_e < n_c/4$ ) region. As discussed below, features around  $670$  to  $680 \text{ nm}$  may plausibly be due to SRS or TPD.

The TPD doublet  $\omega/2$  feature appears most prominently in the planar four-beam experiment [Fig. 3(a)] at the beginning of the laser pulse when the electron temperature is initially low. It is also evident in the planar single-beam experiment [Fig. 3(c)] and the spherical experiment [Fig. 3(e)] when the use of a long-pass filter suppresses much of the SRS signal below  $630 \text{ nm}$  ( $\sim 0.19 n_c$ ), allowing for the

overall neutral density filtering on the streak camera to be reduced and the  $\omega/2$  feature to be revealed.

SRS in the underdense region is observed throughout each experiment. It is strongest in the single-beam planar experiment with a small spot size [Fig. 3(d)], in which only SRS is observed. Some spectra, e.g., Fig. 3(e), show what appears to be the blue TPD  $\omega/2$  feature overlapping with the underdense SRS feature, indicating that some SRS may be occurring in the region where TPD is active. The SRS feature increases with time, while the TPD feature shows a time behavior similar to the redshifted  $\omega/2$  feature. The expected wavelength separation of the redshifted and blueshifted  $\omega/2$  features at  $n_c/4$  can be estimated based on the simulated electron temperature. The wavelength shift of the red  $\omega/2$  feature is  $\Delta\lambda_{\text{nm}} = 3.09 T_{e,\text{keV}}$ .<sup>29</sup> For a temperature of  $T_e \sim 2.8 \text{ keV}$ , the expected wavelength shift is  $\Delta\lambda_{\text{nm}} \sim 8.5 \text{ nm}$ . The blueshifted feature is shifted by a similar magnitude, so that the separation in wavelengths is expected to be  $\sim 15$  to  $20 \text{ nm}$ , as is typically observed in OMEGA 60-beam experiments. This is considerably less than the  $\sim 35 \text{ nm}$  wavelength shift between the redshifted  $\omega/2$  feature and the broad feature at wavelengths around  $670 \text{ nm}$  in many of the spectra, suggesting that additional (SRS) scattered light is likely contributing to the lower-wavelength feature. However, it is plausible that convective TPD at densities below quarter-critical could cause a wavelength shift comparable to the observations.

Ray-tracing calculations<sup>18</sup> based on SRS sidescatter gain<sup>20</sup> indicate that, in the spherical four-beam experiment, SRS scattered light at wavelengths around  $550 \text{ nm}$  [cut off by the long-pass filter in Fig. 3(e)] but observed in other experiments without that filter] originates from the far wing of the beam farthest from SABS (beam 3) and consists largely of sidescatter (i.e., scattered light perpendicular to the local density contour) with a gain  $G \sim 15$ .<sup>18</sup> The component of the SRS spectrum closer to  $640 \text{ nm}$  is mostly from the beam that contains SABS (Beam 4) and can be collected due to refraction. This signal consists of sidescatter from the wing of that beam with  $G \sim 10$ , and backscatter, while possible, was not calculated to have significant gain.<sup>18</sup> Convective SRS may contribute to SRS observations below  $650 \text{ nm}$  as well.



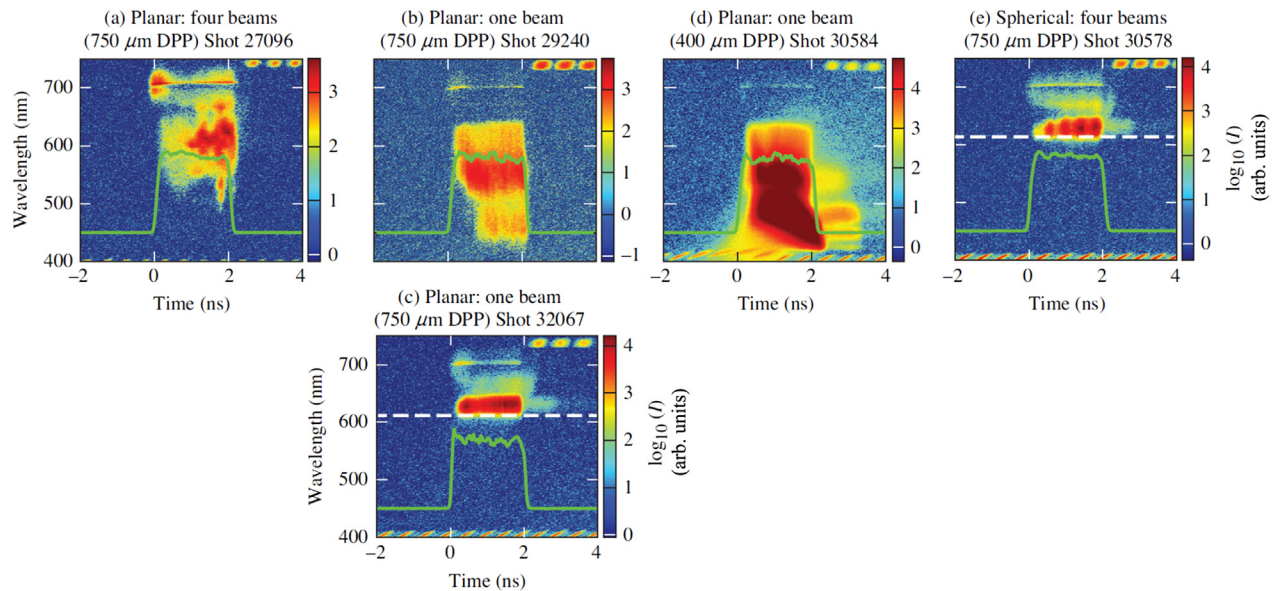


**FIG. 3.** SABS-measured time-resolved scattered light spectra (logarithmic color scale) for experiments with a 2-ns square pulse (green line) and (a) a planar target, irradiated by four beams, (b) and (c) a planar target irradiated by one beam with a  $750\ \mu\text{m}$  spot size, (d) a planar target irradiated by one beam with a  $400\ \mu\text{m}$  spot size, and (e) a  $700\text{-}\mu\text{m}$ -diameter spherical target irradiated by four beams. The dashed white line [(c) and (e)] represents the  $630\ \text{nm}$  cutoff of a long-pass filter, with (b) showing data from a nominally identical experiment as (c), but without the long-pass filter. Periodic features at the top and bottom of the displayed spectra are timing fiducials. The green line represents the laser pulse. The signal is strongly saturated in the  $450\text{--}550\ \text{nm}$  range in (d), with signal after the laser turns off an artifact of the saturation in the streak camera. Different neutral density filtering and SABS throughput for each shot limit comparison of absolute signal levels. Note that (e) was previously shown in and reproduced with permission from Hironaka *et al.*, Phys. Plasmas **30**, 022708 (2023). Copyright 2023 AIP Publishing.<sup>18</sup>

Notably, a linear gain can be estimated from temporal modulation in the underdense SRS spectrum [evident, for example, in Fig. 3(e)] in comparison with a 2.5-GHz modulation inherent in the laser drive. For a four-beam planar experiment with a ramp pulse, the relative modulation amplitude of the single-beam power was  $\sim 5\%$ . The modulation amplitude in the underdense SRS scattered light, after dividing out the exponential increase in SRS reflectivity during the pulse, was  $\sim 60\%$ . Therefore, the gain is estimated to be  $G \sim 12$ , roughly consistent with the calculated SRS sidescatter gains.

The “Raman gap” between underdense and near- $n_c/4$  SRS features is particularly notable at early time in Fig. 3(e) and similar to what was observed in NIF planar experiments.<sup>11,13</sup> The prominent SRS reflectivity in the spherical experiments may also be partially explained by the curvature of isodensity contours, whereby the wings of the beams interact with blow-off plasma from the side of the solid sphere and experience effectively longer scale lengths than at the front of the sphere where the beams overlap [i.e., conditions shown in Figs. 2(e)–2(i)], which is then more susceptible to SRS.

#### IV. DISCUSSION

The data, in contrast to prior results from OMEGA and NIF planar and spherical experiments, elucidate the effect of scale length and single-beam vs overlapped intensity on the prevalence of SRS and TPD.

Most notably, spherical-geometry 60-beam experiments on OMEGA, at scale lengths ( $150\text{--}180\ \mu\text{m}$ ) comparable to the spherical OMEGA EP experiments described here, show evidence only of TPD and do not typically generate SRS signal at overlapped intensities in

the range of these experiments.<sup>8</sup> Though three-dimensional particle-in-cell simulations<sup>31</sup> of LPI for OMEGA-relevant conditions show growth of absolute TPD and SRS instabilities in the same region near the quarter-critical density and that the saturation of both instabilities and the generation of hot electrons are accurately described only with the full nonlinear model including both instabilities, in experiments both SRS and TPD have typically been observed on OMEGA only at much higher intensities ( $\sim 4 \times 10^{15}\ \text{W}/\text{cm}^2$ ) relevant to shock ignition.<sup>30</sup> One key difference between typical OMEGA spherical experiments and the OMEGA EP experiments described here is the single-beam intensities, which are lower ( $\leq 10^{14}\ \text{W}/\text{cm}^2$ ) in OMEGA implosions, where there are typically  $\sim 8$  beams overlapping on a given spot. The appearance of SRS in OMEGA EP experiments at comparable scale length, temperature, and overlapped intensity [Fig. 3(e)], but higher single-beam intensity, indicates that SRS is less of a multiple-beam process and is more strongly influenced by single-beam intensity than is TPD. In contrast, TPD has been demonstrated theoretically and experimentally, including on OMEGA, to occur through multi-beam mechanisms.<sup>17,32,33</sup>

In addition, the small-phase-plate planar experiment likewise achieved a scale length around  $190\ \mu\text{m}$ , roughly comparable to OMEGA and OMEGA EP spherical experiments, but shows different LPI physics. This experiment has an even higher single-beam intensity ( $\sim 4 \times 10^{14}\ \text{W}/\text{cm}^2$ ), despite a lower total overlapped intensity, and shows an overwhelming SRS signal, especially from the underdense region, relative to TPD [Fig. 3(d)]. This experiment is not affected by blowby and is further evidence of the strong single-beam dependence of SRS. In contrast, the planar experiment at  $300\ \mu\text{m}$  scale length

[Fig. 3(a)], driven by four beams and therefore at a modest single-beam intensity, shows considerably more TPD signal in comparison with underdense SRS. The overlapped laser intensity in this four-beam experiment is further above the TPD intensity threshold<sup>16</sup> for absolute single plane wave beams than the single-beam experiment with a small phase plate, by a factor of 3.7 vs by a factor of 1.6. At the same time, the single-beam intensities are at a similar level compared to the absolute SRS threshold,<sup>28</sup> exceeding by a factor of 1.7 for the four-beam experiment and a factor of 1.8 for the single-beam, small phase plate experiment. The high single-beam intensity overcomes the reduced scale length in favoring SRS over TPD in the near-quarter-critical region for the single-beam experiment with the small phase plate, while TPD is relatively more pronounced in the four-beam experiment. Notably, for the four-beam planar and spherical experiments that show evidence of TPD, the TPD threshold is not exceeded when only single-beam intensities are considered (the threshold parameter being reduced by a factor of 4), suggesting a multi-beam origin.

Planar experiments on the NIF at scale lengths of 500–600 μm, driven by 32 to 64 beams (divided into groups of four closely clustered beams denoted “quads”), instead show only evidence of SRS both at the quarter-critical density and in the underdense region.<sup>11,13</sup> Spherical-geometry experiments on NIF, driven in polar-direct-drive geometry, likewise only show evidence of SRS.<sup>12</sup> These long scale lengths are also sufficient to favor SRS over TPD despite modest single-quad intensities in the ~ 10<sup>14</sup> W/cm<sup>2</sup> range as the SRS threshold is a factor of 3 lower than the TPD threshold.<sup>34</sup>

Absolute SRS backscatter thresholds are cited to explain the trends in SRS observations at densities both at and below  $n_c/4$ , including sidescatter, due, in part, to the fact that absolute sidescatter merges continuously into absolute backscatter as the density approaches  $n_c/4$  and the absolute threshold for sidescatter is identical to backscatter for normal incidence at  $n_c/4$ .<sup>35</sup> This threshold intensity also has the same scaling with density scale length as backscatter ( $L^{-4/3}$ ) and only differs, being lower, by a factor of order unity. This means that the absolute threshold for sidescatter is lower than that for backscatter by a factor of ~2, supporting the conclusions on the role of beam overlap and scale length on the relative observed prominence of SRS and TPD. The convective threshold ( $2\pi$  gain) for SRS backscatter occurs for an intensity of a few times 10<sup>15</sup> W/cm<sup>2</sup> for a scale length of 200 μm and is 10% lower if the angle of incidence is increased from normal to 23.2°.

This means that convective backscatter is likewise estimated to be at or below threshold. The modifications in the sidescatter convective gain<sup>20</sup> lead to an enhancement that depends on the density and the plasma wave damping rate. A correct estimation requires detailed ray tracing to be performed, which is beyond the scope of this work. However, this enhancement can easily be factors of two or three, such that gains of 10–20 are possible.

Overlapped laser beam polarization may also play a role in the multi-beam experiment results, as the four beams on OMEGA EP have nearly the same polarization (vertical, modified only by the 23.2° difference in incidence angle), which enhances the multi-beam cooperation between different beams for SRS. In contrast, on OMEGA polarization smoothing is typically applied, and on NIF each quad contains two beams polarized vertically and two beams polarized horizontally with respect to the beam propagation direction. The effect of polarization on SRS, including sidescatter, may be explored in upcoming experiments on the Laser Mégajoule (LMJ) facility.<sup>36</sup>

SRS and TPD observations at different scale lengths and intensities are summarized in Table I. Overall, there is a trend, as observed previously,<sup>11,37</sup> of increasing prevalence of SRS with increasing density scale length. However, the OMEGA EP experiments show that small scale length conditions can also produce significant SRS at both  $n_c/4$  and the underdense region if single-beam intensities are sufficiently high, likely because conditions are approaching or exceeding the convective SRS threshold for a single beam. This result corroborates previous observations of SRS in short-scale length, high-intensity experiments relevant to shock ignition.<sup>38,39</sup> The strongest TPD signals on OMEGA EP are observed in experiments with four overlapping beams, while SRS is most pronounced in single-beam experiments. Overall, these results point to SRS being more of a single-beam phenomenon, while TPD is largely dependent on the superimposition of overlapping beams. This finding is consistent with previous modeling and theoretical examination of SRS and TPD absolute instability thresholds.<sup>16,17,34</sup>

V. CONCLUSIONS

In conclusion, stimulated Raman scattering and two-plasmon decay have been explored systematically in planar and spherical geometries on OMEGA EP, revealing the effects of density scale length, laser intensity, and beam overlap. While previous planar experiments on

TABLE I. Summary of SRS and TPD observations on OMEGA, OMEGA EP, and NIF, as a function of experimental geometry, number of beams, density scale length, electron temperature ( $T_e$ ), and total overlapped and single-beam (for NIF, single-quad) intensities at quarter-critical density, based on 2D DRACO simulations.

Facility	Experiment geometry	# beams	Scale length (μm)	$T_e$ (keV)	Overlapped intensity (W/cm <sup>2</sup> )	Single-beam/quad intensity (W/cm <sup>2</sup> )	LPI observations
OMEGA	Spherical	60	150–180	2.0–2.8	$4\text{--}7 \times 10^{14}$	$0.5\text{--}0.9 \times 10^{14}$	TPD only <sup>8</sup>
OMEGA	Spherical	60	120	3.5	$4 \times 10^{15}$	$5 \times 10^{14}$	TPD and SRS <sup>30</sup>
OMEGA EP	Spherical	4	150	2.7	$8.5 \times 10^{14}$	$2.1 \times 10^{14}$	TPD and SRS
OMEGA EP	Planar	4	300	2.8	$8 \times 10^{14}$	$2 \times 10^{14}$	TPD and SRS
OMEGA EP	Planar	1	190	2	$4 \times 10^{14}$	$4 \times 10^{14}$	Mostly SRS
OMEGA EP	Planar	1	220	1.7	$1.7 \times 10^{14}$	$1.7 \times 10^{14}$	Mostly SRS
NIF	Spherical	192	420	3–3.5	$4\text{--}5 \times 10^{14}$	$0.5\text{--}1.2 \times 10^{14}$	SRS only <sup>12</sup>
NIF	Planar	32–64	500–600	3–4.5	$5\text{--}15 \times 10^{14}$	$0.5\text{--}1.5 \times 10^{14}$	SRS only <sup>11,13</sup>

OMEGA EP, for which scattered light diagnostics were unavailable, were assumed to produce solely TPD,<sup>15</sup> the present experiments clearly identify a regime where TPD and SRS can coexist at densities around and below quarter-critical. As revealed in conjunction with previous experiments on OMEGA and NIF, short density scale lengths and more overlapping beams favor TPD, while longer scale lengths and higher single-beam laser intensities are relatively more favorable for SRS, as high single-beam laser intensities can produce copious SRS both near quarter-critical density and in the underdense region even at short scale lengths. These results are generally consistent with absolute LPI threshold considerations and contribute to further understanding of near-quarter-critical LPI at conditions relevant to direct-drive ICF. These experiments will help guide hot electron preheat mitigation strategies, such as the use of buried Si layers,<sup>40</sup> that may rely on tailoring mitigation techniques to suppress LPI at different locations in the density profile.

## ACKNOWLEDGMENTS

The authors thank OMEGA EP operations and target fabrication for their assistance in executing these experiments. This material is based upon work supported by the Department of Energy National Nuclear Security Administration under Award No. DE-NA0003856, the University of Rochester, and the New York State Energy Research and Development Authority.

This report was prepared as an account of work sponsored by an agency of the U.S. Government. Neither the U.S. Government nor any agency thereof, nor any of their employees, makes any warranty, express or implied, or assumes any legal liability or responsibility for the accuracy, completeness, or usefulness of any information, apparatus, product, or process disclosed, or represents that its use would not infringe privately owned rights. Reference herein to any specific commercial product, process, or service by trade name, trademark, manufacturer, or otherwise does not necessarily constitute or imply its endorsement, recommendation, or favoring by the U.S. Government or any agency thereof. The views and opinions of authors expressed herein do not necessarily state or reflect those of the U.S. Government or any agency thereof.

We acknowledge the support of the Natural Sciences and Engineering Research Council of Canada (NSERC) [Funding Reference Nos. RGPIN-2018-05787 and RGPAS-2018-522497]. Some simulations were performed using resources made available through Compute Canada.

## AUTHOR DECLARATIONS

### Conflict of Interest

The authors have no conflicts to disclose.

### Author Contributions

**Michael Jonathan Rosenberg:** Conceptualization (equal); Data curation (equal); Formal analysis (equal); Investigation (equal); Project administration (equal); Writing – original draft (lead); Writing – review & editing (lead). **Shihui Cao:** Methodology (equal); Software (equal). **Pierre Michel:** Conceptualization (equal). **Mingsheng Wei:** Conceptualization (equal). **John Patrick Palastro:** Conceptualization (equal); Supervision (equal). **Robbie H. H. Scott:** Conceptualization

(equal); Writing – review & editing (equal). **Kevin Glize:** Conceptualization (equal); Software (equal); Writing – review & editing (equal). **Sean Patrick Regan:** Resources (equal); Supervision (equal). **Andrey A. Solodov:** Conceptualization (equal); Data curation (equal); Investigation (equal); Methodology (equal); Software (equal); Writing – original draft (equal); Writing – review & editing (equal). **Jason Frank Myatt:** Conceptualization (equal); Formal analysis (equal); Methodology (equal); Resources (equal); Software (equal); Supervision (equal); Writing – original draft (equal); Writing – review & editing (equal). **Steven Hironaka:** Formal analysis (equal); Methodology (equal); Software (equal). **Janukan Sivajeyan:** Formal analysis (equal); Methodology (equal); Software (equal). **Russell K. Follett:** Conceptualization (equal); Formal analysis (equal); Methodology (equal); Software (equal); Writing – review & editing (equal). **Timothy Filkins:** Data curation (equal); Investigation (equal); Methodology (equal). **Andrei Maximov:** Conceptualization (equal); Writing – review & editing (equal). **Chuang Ren:** Conceptualization (equal); Software (equal); Supervision (equal); Writing – review & editing (equal).

## DATA AVAILABILITY

The data that support the findings of this study are available from the corresponding author upon reasonable request.

## REFERENCES

- W. L. Kruer, *The Physics of Laser Plasma Interactions* (Addison-Wesley, Redwood City, CA, 1988).
- S. Atzeni and J. Meyer-Ter-Vehn, *The Physics of Inertial Fusion: Beam Plasma Interaction, Hydrodynamics, Hot Dense Matter*, International Series of Monographs on Physics (Clarendon, Oxford, 2004).
- R. P. Drake, R. E. Turner, B. F. Lasinski, K. G. Estabrook, E. M. Campbell, C. L. Wang, D. W. Phillion, E. A. Williams, and W. L. Kruer, *Phys. Rev. Lett.* **53**, 1739 (1984).
- W. Seka, E. A. Williams, R. S. Craxton, L. M. Goldman, R. W. Short, and K. Tanaka, *Phys. Fluids* **27**, 2181 (1984).
- H. Figueroa, C. Joshi, H. Azechi, N. A. Ebrahim, and K. Estabrook, *Phys. Fluids* **27**, 1887 (1984).
- A. Simon, R. W. Short, E. A. Williams, and T. Dewandre, *Phys. Fluids* **26**, 3107 (1983).
- C. A. Haynam, P. J. Wegner, J. M. Auerbach, M. W. Bowers, S. N. Dixit, G. V. Erbert, G. M. Heestand, M. A. Henesian, M. R. Hermann, K. S. Jancaitis, K. R. Manes, C. D. Marshall, N. C. Mehta, J. Menapace, E. Moses, J. R. Murray, M. C. Nostrand, C. D. Orth, R. Patterson, R. A. Sacks, M. J. Shaw, M. Spaeth, S. B. Sutton, W. H. Williams, C. C. Widmayer, R. K. White, S. T. Yang, and B. M. V. Wonterghem, *Appl. Opt.* **46**, 3276 (2007).
- W. Seka, D. H. Edgell, J. F. Myatt, A. V. Maximov, R. W. Short, V. N. Goncharov, and H. A. Baldis, *Phys. Plasmas* **16**, 052701 (2009).
- R. S. Craxton, K. S. Anderson, T. R. Boehly, V. N. Goncharov, D. R. Harding, J. P. Knauer, R. L. McCrory, P. W. McKenty, D. D. Meyerhofer, J. F. Myatt *et al.*, *Phys. Plasmas* **22**, 110501 (2015).
- T. R. Boehly, D. L. Brown, R. S. Craxton, R. L. Keck, J. P. Knauer, J. H. Kelly, T. J. Kessler, S. A. Kumpan, S. J. Loucks, S. A. Letzring *et al.*, *Opt. Commun.* **133**, 495 (1997).
- M. J. Rosenberg, A. A. Solodov, J. F. Myatt, W. Seka, P. Michel, M. Hohenberger, R. W. Short, R. Epstein, S. P. Regan, E. M. Campbell, T. Chapman, C. Goyon, J. E. Ralph, M. A. Barrios, J. D. Moody, and J. W. Bates, *Phys. Rev. Lett.* **120**, 055001 (2018).
- M. Hohenberger, P. B. Radha, J. F. Myatt, S. LePape, J. A. Marozas, F. J. Marshall, D. T. Michel, S. P. Regan, W. Seka, A. Shvydky *et al.*, *Phys. Plasmas* **22**, 056308 (2015).



- <sup>13</sup>M. J. Rosenberg, A. A. Solodov, W. Seka, R. K. Follett, J. F. Myatt, A. V. Maximov, C. Ren, S. Cao, P. Michel, M. Hohenberger, J. P. Palastro, C. Goyon, T. Chapman, J. E. Ralph, J. D. Moody, R. H. H. Scott, K. Glize, and S. P. Regan, *Phys. Plasmas* **27**, 042705 (2020).
- <sup>14</sup>L. J. Waxer, D. N. Maywar, J. H. Kelly, T. J. Kessler, B. E. Kruschwitz, S. J. Loucks, R. L. McCrory, D. D. Meyerhofer, S. F. B. Morse, C. Stoeckl, and J. D. Zuegel, *Opt. Photonics News* **16**(7), 30–36 (2005).
- <sup>15</sup>D. T. Michel, A. V. Maximov, R. W. Short, S. X. Hu, J. F. Myatt, W. Seka, A. A. Solodov, B. Yaakobi, and D. H. Froula, *Phys. Rev. Lett.* **109**, 155007 (2012).
- <sup>16</sup>C. Z. Xiao, H. B. Zhuo, Y. Yin, Z. J. Liu, C. Y. Zheng, and X. T. He, *Nucl. Fusion* **60**, 016022 (2020).
- <sup>17</sup>R. K. Follett, J. G. Shaw, J. F. Myatt, D. H. Froula, and J. P. Palastro, *Phys. Rev. E* **101**, 043214 (2020).
- <sup>18</sup>S. Hironaka, J. Sivajeyan, J. Wang, M. J. Rosenberg, A. Solodov, T. Filkins, C. Xiao, Q. Wang, W. Seka, and J. F. Myatt, *Phys. Plasmas* **30**, 022708 (2023).
- <sup>19</sup>S. Depierreux, C. Neuville, C. Baccou, V. Tassin, M. Casanova, P.-E. Masson-Laborde, N. Borisenko, A. Orekhov, A. Colaitis, A. Debayle *et al.*, *Phys. Rev. Lett.* **117**, 235002 (2016).
- <sup>20</sup>P. Michel, M. J. Rosenberg, W. Seka, A. A. Solodov, R. W. Short, T. Chapman, C. Goyon, N. Lemos, M. Hohenberger, J. D. Moody, S. P. Regan, and J. F. Myatt, *Phys. Rev. E* **99**, 033203 (2019).
- <sup>21</sup>T. Filkins *et al.*, *Rev. Sci. Instrum.* (in press).
- <sup>22</sup>W. Seka, J. F. Myatt, R. W. Short, D. H. Froula, J. Katz, V. N. Goncharov, and I. V. Igumenshchev, *Phys. Rev. Lett.* **112**, 145001 (2014).
- <sup>23</sup>P. B. Radha, V. N. Goncharov, T. J. B. Collins, J. A. Delettrez, Y. Elbaz, V. Y. Glebov, R. L. Keck, D. E. Keller, J. P. Knauer, J. A. Marozas *et al.*, *Phys. Plasmas* **12**, 032702 (2005).
- <sup>24</sup>J. A. Marozas, F. J. Marshall, R. S. Craxton, I. V. Igumenshchev, S. Skupsky, M. J. Bonino, T. J. B. Collins, R. Epstein, V. Y. Glebov, D. Jacobs-Perkins, J. P. Knauer, T. C. Sangster, W. Seka, and V. A. Smalyuk, *Phys. Plasmas* **13**, 056311 (2006).
- <sup>25</sup>D. Cao, G. Moses, and J. Delettrez, *Phys. Plasmas* **22**, 082308 (2015).
- <sup>26</sup>G. P. Schurtz, P. D. Nicolaï, and M. Busquet, *Phys. Plasmas* **7**, 4238 (2000).
- <sup>27</sup>W. F. Huebner, A. L. Merts, N. H. Magee Jr., and M. F. Argo, Report No. LA-6760-M (Los Alamos National Laboratory, Los Alamos, NM, 1977).
- <sup>28</sup>C. S. Liu, M. N. Rosenbluth, and R. B. White, *Phys. Fluids* **17**, 1211 (1974).
- <sup>29</sup>W. Seka, B. B. Afeyan, R. Boni, L. M. Goldman, R. W. Short, K. Tanaka, and T. W. Johnston, *Phys. Fluids* **28**, 2570 (1985).
- <sup>30</sup>W. Theobald, R. Nora, W. Seka, M. Lafon, K. S. Anderson, M. Hohenberger, F. J. Marshall, D. T. Michel, A. A. Solodov, C. Stoeckl, D. H. Edgell, B. Yaakobi, A. Casner, C. Reverdin, X. Ribeyre, A. Shvydky, A. Vallet, J. Peebles, F. N. Beg, M. S. Wei, and R. Betti, *Phys. Plasmas* **22**, 056310 (2015).
- <sup>31</sup>H. Wen, A. V. Maximov, R. Yan, J. Li, C. Ren, and F. S. Tsung, *Phys. Rev. E* **100**, 041201 (2019).
- <sup>32</sup>J. R. Fein, J. P. Holloway, M. R. Trantham, P. A. Keiter, D. H. Edgell, D. H. Froula, D. Haberberger, Y. Frank, M. Fraenkel, E. Raicher *et al.*, *Phys. Plasmas* **24**, 032707 (2017).
- <sup>33</sup>R. K. Follett, J. F. Myatt, J. G. Shaw, D. T. Michel, A. A. Solodov, D. H. Edgell, B. Yaakobi, and D. H. Froula, *Phys. Plasmas* **24**, 102134 (2017).
- <sup>34</sup>Q. Wang, W. Rozmus, and J. F. Myatt, *Phys. Plasmas* **28**, 122711 (2021).
- <sup>35</sup>B. B. Afeyan and E. A. Williams, *Phys. Fluids* **28**, 3397 (1985).
- <sup>36</sup>J.-L. Miquel, C. Lion, and P. Vivini, *J. Phys.: Conf. Ser.* **688**, 012067 (2016).
- <sup>37</sup>R. H. H. Scott, K. Glize, L. Antonelli, M. Khan, W. Theobald, M. Wei, R. Betti, C. Stoeckl, A. G. Seaton, T. D. Arber, D. Barlow, T. Goffrey, K. Bennett, W. Garbett, S. Atzeni, A. Casner, D. Batani, C. Li, and N. Woolsey, *Phys. Rev. Lett.* **127**, 065001 (2021).
- <sup>38</sup>G. Cristoforetti, A. Colaitis, L. Antonelli, S. Atzeni, F. Baffigi, D. Batani, F. Barbato, G. Boutoux, R. Dudzak, P. Koester, E. Krousky, L. Labate, P. Nicolaï, O. Renner, M. Skoric, V. Tikhonchuk, and L. A. Gizzi, *Europhys. Lett.* **117**, 35001 (2017).
- <sup>39</sup>G. Cristoforetti, L. Antonelli, D. Mancelli, S. Atzeni, F. Baffigi, F. Barbato, D. Batani, G. Boutoux, F. D'Amato, J. Dostal *et al.*, *High Power Laser Sci. Eng.* **7**, e51 (2019).
- <sup>40</sup>A. A. Solodov, M. J. Rosenberg, M. Stoeckl, A. R. Christopherson, R. Betti, P. B. Radha, C. Stoeckl, M. Hohenberger, B. Bachmann, R. Epstein, R. K. Follett, W. Seka, J. F. Myatt, P. Michel, S. P. Regan, J. P. Palastro, D. H. Froula, E. M. Campbell, and V. N. Goncharov, *Phys. Rev. E* **106**, 055204 (2022).